Chapter 1

Introduction

1.1 Fundamental structure of matter

The fundamental research in physics evolves the understanding of mankind at a great rate in the last century. The everlasting hunt to determine what are we made of or what is the fundamental structure of matter has led to a broadly adopted classification of fundamental particles. In the course of time, physicists become triumphant in portraying matter to be made up of some smaller entities. The origin of today's world is supposed to be the so called big bang, during which time, space, matter and energy emerged as reality. In ancient time it was believed that there were four set of classical elements: earth, water, air, and fire; sometimes including a fifth element called aether in ancient Greece and akasha in India [1]. The idea of the five elements established a background of analysis in both Hinduism and Buddhism. This theory of classical elements prevailed to the seventeenth century until the beginning of the modern chemistry when the great chemist Robert Boyle gave the new definition for an element. About a hundred years later the British chemist John Dalton proposed the modern atomic theory in 1809 and gave a list of elements that is a clear outrider to today's tabulation of the hundred and more elements. In 1897, the first subatomic particle called the electron was discovered by Joseph John Thomson. The discovery of proton by Ernest Rutherford in 1911 in his famous scattering experiment superseded Thomsons plum pudding model of the atom. Later in 1932 Rutherford's student James Chadwick discovered the neutron following which the detailed picture of atomic nuclei was undocked.

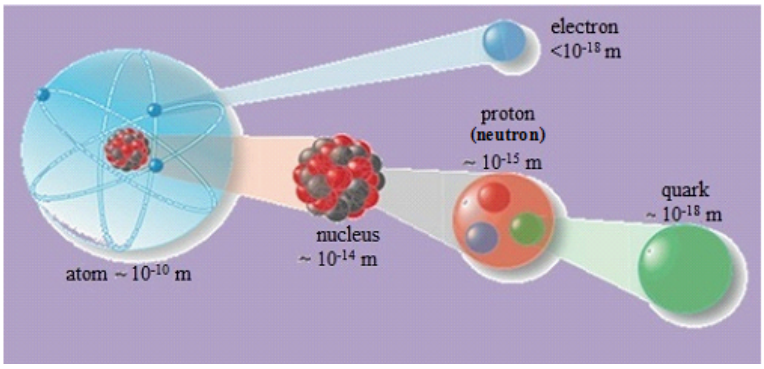

Figure 1.1: The structure within the atom

By the 1960s more and more new particles like proton and neutron, called hadrons, were discovered and it was justifiable to admit that the strongly bound hadrons were not truly fundamental particles, but were composed of some further anonymous elementary entities. In 1964 Murray Gell-mann and George Zweig independently proposed that these entities were a family of spin 1/2 particles which they named quarks [2, 4] and according to their theory each hadron was consisted of either three quarks, known as baryons, or a quark and anti-quark pair, known as mesons. Then, in 1968, the high energy electron-proton scattering experiments at the Stanford Linear Accelerator Center (SLAC) revealed the existence of hard scattering centers inside the proton, thus confirming, undoubtedly, that it surely was a composite particle. Richard Feynman in 1969 proposed the parton model in which the hadrons were supposed to be composite objects of some more fundamental particles, the so-called partons [5]. Later it was identified that these partons represent the same objects nowadays usually referred to as 'quarks' and 'gluons'. The main difference between Rutherford's experiment and the electron-proton scattering experiments comes from the fact that, the dimension of an atom is typically 10^{-10} m whereas that of a proton is about 1 fm = 10^{-15} m (Figure 1.1). From the uncertainty principle $\Delta E.\Delta x \geq hc \approx 0.2$ GeVfm, it is clear that the smaller the distance to be probed the higher must be the beam energy. The probing inside the proton ($x << 1$ fm) requires a beam energy $E >> 1$ GeV. The requirement of this high energy acceleration technique is responsible for more than 50 years gap between the two experiments.

The quark model possessed various puzzling features regardless of its achievement that included the probable absence of isolated quarks as well as two quark (qq) or

four quark combinations (qqqq). Over the past decade, however, particle-accelerator activities all over the world have assembled some indication that a few different kinds of four-quark particles might exist. Very recently using the most powerful particle collider in the world, the Large Hadron Collider (LHC), a research group at CERN has produced a particle made of four quarks go by the name $Z(4430)^-$ [6]. They exist only in exceedingly high-energy ambiance for an extremely short period of time. Moreover the presence of pentaquark states was announced by various experiments in the middle of the year 2000, but subsequent experiments and reanalysis of the data revealed them to be statistical effects instead of true resonances. A further problem was associated with the Δ^{++} baryon as the quantum numbers of this particle turned out to violate the Pauli exclusion principle. These enigmas were sooner or later resolved by the addition of another degree of freedom referred to as color and to that end along with all other quantum numbers quarks also carry a color charge. Nevertheless due to color confinement all particles observed in nature must be color singlet, and so the only permissible quark combinations appear to be simply the three quarks or three antiquarks as well as a quark and an antiquark compositions.

Our current understanding of the basic building blocks of matter and how do they interact with each other can be explained by a theory, known as the Standard Model (SM) [6-9]. Over time and through many experiments, physicists have successfully developed the SM into a well-tested theory of particle physics that marks a milestone in our present knowledge on what the world is and what holds it together. It was flourished during the latter half of the 20th century, as a joint endeavor of scientists throughout the world. The present formulation was established in the middle of 1970s consequent to the experimental evidence for the existence of quarks. Ever since the discoveries of the W and Z bosons in 1981 [10], the top quark in 1995 [11], the tau neutrino in 2000 [12], and more recently the Higgs boson with spin 0, the first elementary scalar particle ever discovered in nature, in 2012 [13] at the worlds largest particle accelerator, the CERN's Large Hadron Collider (LHC) have added further credibility to the already established SM. According to this theory, the most fundamental building blocks of all matter in the universe are quarks and leptons along with their antiparticles. Nonetheless, the experiments colliding beam of protons at the highest LHC energies will be awaiting to see whether quarks themselves contain

more fundamental constituents. Each of these particles comes in six distinct types and their interactions are mediated by the force carrier particles. The particles that make up ordinary matter i.e. leptons and quarks are fermions, whereas the force carriers are bosons. The six quarks form three doublets of the electroweak symmetry group SU(2).

The SM organizes the elementary particles into three generations, including two quarks and two leptons in each generation as shown in Figure 1.2. Particles in generation I are less massive than those in generation II, which are less massive than those in generation III. The up quark, the down quark, the electron and the electron neutrino are placed in the first generation; the second generation includes the charm quark, the strange quarks, the muon and the muon neutrino; while the third generation consists of the top and bottom quarks and the tau and tau neutrino. The ordinary matter, for example the stable atoms made of electrons, protons, and neutrons with effectively infinite life spans, is exclusively made up of first-generation particles. Being heavier higher generations particles quickly disintegrate into first-generation particles, and thus are not usually experienced. The hadron with longest life time containing a second generation quark is the lambda particle, made of an up, down, and strange quark. It has a mean lifetime less than a billionth of a second, which is comparatively long-lasting for an unstable hadron. Particles of third generation are divided according to their behavior. The bottom quark does not differ much from a strange quark. On the other hand the top quark is very short-lived and breaks down before anything realizes its existence. They can only be recognized from their decay products.

There are four fundamental forces in the universe: the strong force, the electromagnetic force, the weak force and the gravitational force. The SM includes the electromagnetic, strong and weak forces and all their carrier particles, and explains well how these forces act on all of the matter particles. However, the most familiar force in our everyday lives, gravity, is not a part of the SM. The weak and strong forces are effective only over a very short range and dominate only at the level of subatomic particles whereas the electromagnetic force acts over an infinite range. Gravity is the weakest of the four fundamental forces and appears to have infinite range unlike the strong or weak force. It is speculated that the gravitational force is mediated

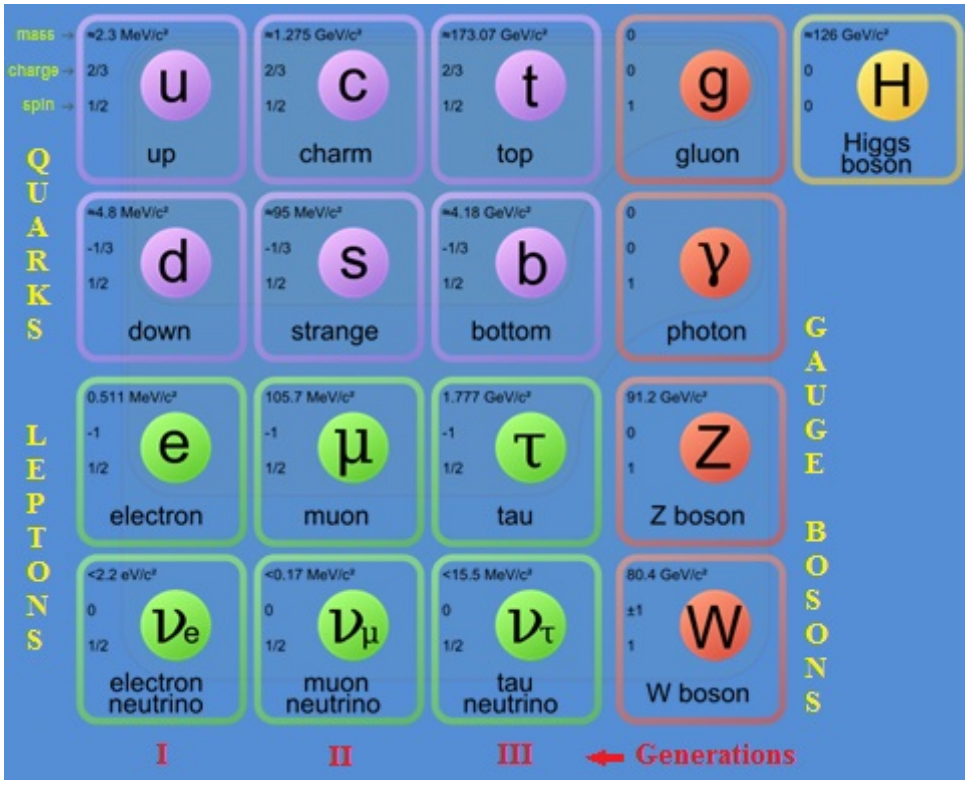

Figure 1.2: Standard model of elementary particles

by a massless spin-2 particle called the graviton, yet to be discovered. The LHC experiments could give indication for extra dimensions apart from the four dimensions we experience and allow the study of higher-dimensional gravitons. Nevertheless, some theories predict that high-energy experiments at LHC could create gravitons escaping into the extra dimensions. Quantum electrodynamics (QED), a quantum field theory, mathematically describes all phenomena involving electrically charged particles, interacting by means of exchange of photon, the massless, uncharged, spin 1 gauge boson. The weak interaction is accountable for both the radioactive decay and nuclear fusion of subatomic particles. The weak interaction affects all the fermions of the SM, as well as the Higgs boson and is mediated by two massive gauge bosons: the charged $W^{\pm}$ or the neutral Z^0, also known as intermediate vector bosons. Neutrinos are the only particles to feel just one of the fundamental forces, the weak interaction, which is what makes them so hard to investigate. The weak interaction is best understood in terms of Glashow, Salam, and Weinbergs electro-weak theory (EWT) which unifies both the weak and electromagnetic forces into one at higher energies [7-9].

The strong force, as the name implies, is the strongest of all four fundamental

interactions. Quarks and gluons are the only fundamental particles that carry color charge, and hence participate in strong interactions. The quantum field theory that describes strong interactions is named as Quantum Chromodynamics (QCD) for this property of color. The strong interactions among the quarks are exchanged by gluons, the massless gauge boson with spin 1, like photons. However, unlike photons, which are not electrically charged and therefore do not feel the electromagnetic force, gluons do take part in strong interaction and can interact among themselves. But the behavior of this crucial, prevalent binding force is exceptionally difficult to understand. A new electron-ion collider (EIC) [14] could successfully unfold the enigmas of the glue. Within short range about 10^{-15} metre, approximately the diameter of a proton or a neutron, the strong force becomes stronger with distance, unlike the other forces. However, the strong force between quarks becomes weaker at short distances. That is Quarks behave independently when they are close, but they can not be pulled apart. Due to this property, known as the asymptotic freedom [15-17], the various interactions between the quarks can possibly be neglected when probing the hadron with a high energy particle. Consequently free quarks are not observed in nature but rather they are permanently confined within colorless hadrons.

So far so good, but there are many shortcomings in the SM as it fails to explain the complete picture, such as the strong CP problem, neutrino oscillations, matter-antimatter asymmetry, and the dark matter and dark energy etc. Another problem with SM is that it incorporates only three out of the four fundamental forces, omitting gravity. The model is also unsuccessful in explaining why gravity is so much weaker than the electromagnetic or strong forces. Moreover it cannot provide justification for the three generations of quarks and leptons with such a diverse mass scale. The hierarchy problem is also associated with the Higgs boson mass. Last but not the least, the SM only describes visible matter, but it cannot explain the nature of the dark matter and dark energy. Many attempts in the theoretical and experimental physics are going on to extend the SM through supersymmetry or to discard it in favor of new theories like Minimal Supersymmetric Standard Model (MSSM), string theory and extra dimensions. Regardless of the deficiencies, the SM is the most successful theory of particle physics to date.

1.2 Quantum chromodynamics

QCD is the theory that describes the dynamics of the strong interactions between quarks and gluons. Its phenomenological utilizations to a large extent, concerning which people go on learning, are still very interesting topics of active research. QCD is a special case of a non-abelian Yang-Mills theory with the gauge group SU(3), the Special Unitary group in 3 dimensions [18]. This gauge group involves the additional degree of freedom known as color, completely unrelated to the everyday familiar phenomenon of color, which plays an essential part in the dynamics of the theory. The concept of color first originated from the discovery of the Δ^{++} baryon composed of three strange quarks with parallel spins when its quantum numbers seemed to violate the Pauli exclusion principle. The idea of color as the origin of a strong field was evolved into the theory of QCD in the 1970s by the physicists Harald Fritzsch and Heinrich Leutwyler, together with Murray Gell-Mann [19]. According to QCD quarks carry a color charge of red (R), green (G) or blue (B) and antiquarks have a color charge of antired (cyan), antigreen (megenta) and antiblue (yellow) i.e. $\bar{R}$, $\bar{G}$, $\bar{B}$ [18]. Especially, it is of great importance that the gauge bosons of QCD, the gluons, carry color as well and therefore can interact among themselves. In this way apart from the well known fermion-boson vertex, the QCD Lagrangian further involves three-gluon and four-gluon vertices. Figure 1.3 shows the schematic representation of the basic QCD Feynman diagrams. Due to the specific characteristic of gluon self coupling in QCD it is feasible to have a convincing theory including only the gauge fields without any fermion, and so in some situations the contributions arising from only the gauge part are likely to be separated from the fermionic contributions. Moreover the existence of jets in QCD is subjected to these gluon-gluon interactions. Gluons have a combination of a color and an anticolor of a different kind in a superposition of states which are equivalent to the Gell-Mann matrices. Unlike the single photon of QED or the three $W^{\pm}$ and Z^0 bosons of the weak interaction, there are evidently eight kinds of gluons in QCD listed as follows [18]: $R\bar{G}$, $R\bar{B}$, $G\bar{R}$, $G\bar{B}$, $B\bar{R}$, $B\bar{G}$, $(R\bar{R}-G\bar{G})/\sqrt{2}$ and $(R\bar{R}+G\bar{G}-2B\bar{B})/\sqrt{6}$. In other words, the gluons belong to a $SU(3)$ color octet. The remaining combination, the $SU(3)$ color singlet, $(R\bar{R}+G\bar{G}+B\bar{B})/\sqrt{3}$ does not take part in the interaction.

Two outstanding features of QCD are confinement and asymptotic freedom [15-

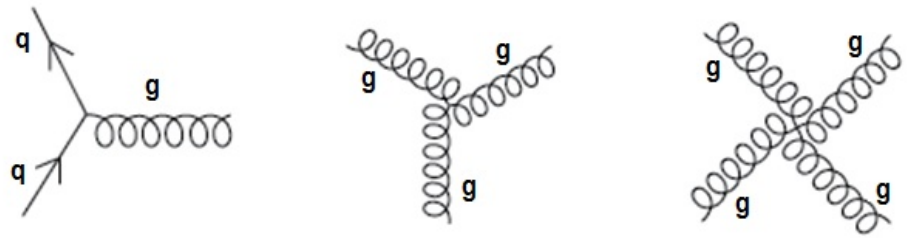

Figure 1.3: Basic QCD Feynmann diagrams

17]. The perturbative analysis of QCD is well grounded based on the fact that the theory is asymptotically free, that is, at short distance the quarks and gluons behave as quasi-free particles whereas at longer distance the force of attraction between quarks and gluons becomes stronger and stronger. Therefore no free color charge has ever been observed in nature, rather they are confined within the experimentally observed color neutral composite states of hadrons. The coupling constant which is a measure of the effectiveness of the strong force that holds quarks and gluons together into composite particles introduces a dependence on the absolute scale, implying more radiation at low scales than at high ones and it is usually referred to as running coupling constant [20]. The running is logarithmic with energy, and is governed by the so-called beta function,

$$\frac{\partial \alpha_s}{\partial \ln (Q^2)} = \beta(\alpha_s), \tag{1.1}$$

where

$$\beta(\alpha_s) \equiv \frac{\partial \alpha_s(Q)^2}{\partial \ln (Q^2)} = -\frac{\beta_0}{4\pi}\alpha_s^2 - \frac{\beta_1}{16\pi^2}\alpha_s^3 - \frac{\beta_2}{64\pi^2}\alpha_S^4 + \mathcal{O}(\alpha_s^5) \tag{1.2}$$

with one-loop, two-loop and three-loop coefficients

$$\beta_0 = \frac{11}{3}N_c - \frac{4}{3}T_f = 11 - \frac{2}{3}N_f,$$

$$\beta_1 = \frac{34}{3}N_c^2 - \frac{10}{3}N_c N_f - 2C_F N_f = 102 - \frac{38}{3}N_f,$$

and

$$\begin{aligned} \beta_2 &= \frac{2857}{54}N_c^3 + 2C_F^2 T_f - \frac{205}{9}C_F N_c T_f - \frac{1415}{27}N_c^2 T_f + \frac{44}{9}C_F T_f^2 + \frac{158}{27}N_c T_f^2 \\ &= \frac{2857}{2} - \frac{6673}{18}N_f + \frac{325}{54}N_f^2. \end{aligned}$$

Here N_f is the number of active fermion flavors and N_c is the number of colors. We use $N_f = 4$, $N_c = 3$, $T_f = \frac{1}{2}N_f$ and $C_F = \frac{N_c^2-1}{2N_c}$, C_F being the color factor associated

with the color group SU(3). Numerically, the value of the strong coupling is usually specified by two parameters, the renormalization scale (μ) and the corresponding value of the coupling at that point, from which we can obtain its value at any other scale from Eq.1.1,

$$\alpha_s(Q^2) = \frac{\alpha_s(\mu^2)}{1 + \alpha_s(\mu^2)\beta_0 \ln(Q^2/\mu^2) + \mathcal{O}(\alpha_s^2)}. \tag{1.3}$$

These two parameters can be replaced for a single parameter Λ so that the running coupling can be expressed as

$$\alpha_s(Q^2) = \frac{1}{\beta_0 \ln(Q^2/\Lambda^2)}. \tag{1.4}$$

The coupling would clearly diverge at the scale Λ, called the Landau pole, which specifies the energy scale at which the perturbative coupling would nominally become infinite. Its value is experimentally found to be $\Lambda \approx 200$ GeV. This implies that the perturbation calculations are allowed only at energy scales of or higher than 1 GeV. Moreover, the structure of hadrons cannot be determined applying perturbation theory as a result of confinement. Alternatively, the quark and gluon content of hadrons are computed by parametrizations of the distribution functions obtained from high energy scattering experiments. Being universal these distribution functions are very useful to make prognostications for other experiments.

1.3 Deep inelastic scattering and structure functions

Deep inelastic scattering (DIS) [21, 22] has long been an excellent tool of exploring the inner structure of a hadron, say proton. DIS provides the first conceivable indication of the reality of quarks which so far had been considered by many to be merely a mathematical fact. In lepton-nucleon DIS for example, electrons and protons are accelerated to very high energies and then allowed them to collide. The four-momentum squared (Q^2) of the exchanged virtual photon in this process determines the resolving power. The spatial resolution with which structure of the proton is probed is roughly the De Broglie wavelength of the virtual photon $\lambda \sim 1/Q$. At large Q^2, the wavelength associated with the electron are much smaller than the size of a proton, thereby resolving smaller distances within the proton, i.e. a single quark

inside the proton scatters off the photon. Thus DIS assist us to extract information on the the parton dynamics and the momentum distributions of quarks and gluons inside the proton to a great extent. Over and above that DIS is solicitous to the discovery and interpretation of new physics which could be observed in extreme conditions of high parton densities at very small Bjorken-x. The first DIS experiments were performed at SLAC in California in 1968 following which a lot of other DIS experiments exploring the proton structure have been carried out until 2007 with the high energy HERA electron-proton collider at DESY in Hamburg. Most recently a new colliding beam facility, the Large Hadron Electron Collider (LHeC) [23], is proposed at CERN for lepton-nucleon scattering which will produce an unprecedented kinematic domain for lepton-nucleon scattering with the centre of mass energy of 1.3 TeV being four times larger than the previous highest attainable energy at HERA. In lepton-nucleon neutral-current (NC) DIS, a neutral boson, i.e. a photon or a Z^0,

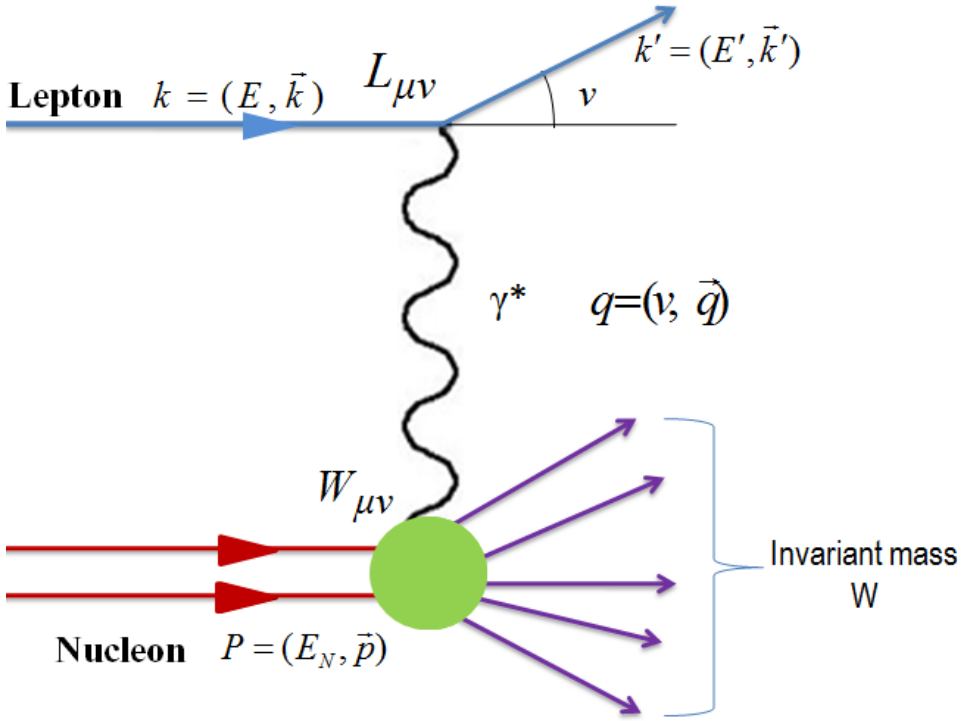

Figure 1.4: Schematic representation of DIS

is exchanged between the electron (or positron) and the quark, in contrast to the charged-current (CC) DIS where a charged $W^{\pm}$ boson is exchanged when a neutrino interacts with a nucleon. The resulting process of DIS is inclusive when this hadronic final state remains undetected, or semi-inclusive when apart from the lepton some

produced hadrons are detected or exclusive when all final products are identified. The basic process of NC DIS where the lepton with four momentum k interacts with the proton with four momentum p through the exchange of a virtual photon whose momentum is q is depicted in Figure1.4. The cross section of the process can be described by the following Lorentz invariant kinematic variables [18]:
Exchanged four momentum squared or virtuality of photon:

$$Q^2 \equiv -q^2 = (k - k');$$

Square of the invariant mass of the final state hadronic jet:

$$W^2 = (p + q)^2 = M^2 + 2p.q + q^2;$$

Center of mass energy squared:

$$s = (p + k)^2;$$

Energy transfer from the lepton to the proton:

$$\nu = p.q;$$

Bjorken scaling variable representing the fracton of proton's four momentum carried by a parton:

$$x = \frac{Q^2}{2\nu} \text{ and}$$

Fraction of energy lost by the electron in the proton rest frame (inelasticity):

$$y = \frac{p.q}{p.k} = 1 - E'/E.$$

Here k denotes the four momentum of the incoming electron and k' the four momentum of the scattered electron, E and E' are the initial and final electron energies in the rest frame of the target proton and M is the mass of the proton. Q^2 and ν are the two independent variables in DIS. The dimensionless x is related to the variables y, Q^2 and s via the approximate relation $Q^2 = xys$. Since the proton is the lightest baryon, therefore $W > M$. It is necessary to measure E, E' and the scattering angle θ in the laboratory reference frame to determine the full kinematics. The aforementioned kinematic variables have a finite range of allowed values: $0 < x < 1$; $0 < y < 1$; $0 < Q^2 < s$ and $M < W < \sqrt{s}$.

The scattering cross section can be splitted into a leptonic part describing the emission of the virtual photon by the lepton and a hadronic part describing the interaction of the virtual photon with the proton,

$$d\sigma \sim L_{\mu\nu} W^{\mu\nu}. \tag{1.5}$$

The most general form of the tensor $W_{\mu\nu}$ can be constructed out of $g^{\mu\nu}$ and independent momenta p and q as

$$W^{\mu\nu} = \Big(g^{\mu\nu} - \frac{q^\mu q^\nu}{q^2}\Big) W_1(x, Q^2) + \Big(p^\mu + \frac{1}{2x} q^\mu\Big)\Big(p^\nu + \frac{1}{2x} q^\nu\Big) W_2(x, Q^2). \tag{1.6}$$

The proton structure function is characterised by two measurable functions W_1 and W_2 or equivalently the so-called structure functions F_1 and F_2:

$$F_1(x, Q^2) = W_1(x, Q^2),$$

$$F_2(x, Q^2) = \nu W_2(x, Q^2). \tag{1.7}$$

Structure functions are the established observables in DIS providing unique information about the deep structure of hadrons as well as their interactions. They allow perturbative QCD to be precisely tested and and to a great degree, they form the backbone of our understanding concerning the parton densities which are indispensable to investigate the hard scattering processes. In terms of F_1 and F_2 the unpolarized DIS cross section can be expressed as

$$\frac{d^2\sigma}{dx dQ^2} = \frac{4\pi\alpha_S^2(Q^2)}{Q^4}\Big[xy^2 F_1(x, Q^2) + (1-y) F_2(x, Q^2)\Big], \tag{1.8}$$

where the first term F_1 corresponds to the absorption of a transversely polarized photon, while the longitudinally polarized component of the cross section is given by $F_L(x, Q^2) = F_2(x, Q^2) - 2xF_1(x, Q^2)$. Further in the limit $Q^2 \to \infty$ and fixed x, any strong interactions among the partons can be neglected and the proton structure functions can be estimated from an incoherent sum of the partons. Then F_1 and F_2 become independent of Q^2 and are functions of the dimensionless kinematical variable x only. This is known as the so-called Bjorken scaling [24]. The well-known SLAC-MIT experiment on DIS observed that the measured DIS cross section exhibit approximate scaling behavior [25]. In the Bjorken limit the quarks in the proton can absorb only the transversely polarized photons, whereas the the longitudinally

polarized photons can not be absorbed due to halicity conservation and therefore the longitudinal part of the cross section turns out to vanish. In that case F_1 and F_2 are related through the famous Callan-Gross relation $2xF_1(x) = F_2(x)$ which is a direct consequence of the existence of point like quarks with spin 1/2 within proton.

QCD extends the naive quark parton model by allowing interactions between the partons via the exchange of gluons. The processes that generate the parton interactions to first order in α_s are gluon radiation ($q \to qg$), gluon splitting ($g \to gg$) and quark pair production ($g \to q\bar{q}$). In DIS, at smaller values of Q^2 the photon can resolve only the valence quarks with relatively large values of x with a finite resolution proportional to $1/Q$. On the other hand, at higher values of Q^2 the photon, having a smaller wavelength, can resolve the quarks at smaller distance scales. Thus in the high Q^2 region gluon radiation leads to the creation of quark-antiquark pairs with relatively small values of x. The parton densities will thus increase with increasing Q^2. Analysis of the cross section shows that this increase mainly occurs at small-x. Therefore, QCD persuades the requirement of an additional scale Q^2 for the representation of the parton densities. Accordingly beyond the bounds of parton model approximation the PDFs and therefore the structure functions come to have a Q^2 dependence through higher order corrections in $\alpha_s(Q^2)$ resulting in sizeable scaling violations [26]. The HERA experiments, H1 and ZEUS [27-30] measured the proton structure function F_2 extensively and perfectly established its scaling violations anticipated by QCD over a wide kinematic region. The predicted scale dependence further enables the factual estimation of $\alpha_s(Q^2)$ as well as provides an explicit verification of QCD.

1.4 Parton distribution functions

Perturbative QCD or any other cross sections involving initial-state hadrons can not provide first-hand appraisal of structure functions owing to the fact that the initial-state particles in the experiments of different high energy collider viz. HERA, Tevatron as well as LHC are not quarks and gluons, but the composite hadrons. Therefore, it is a prerequisite to know the momentum distributions of the partons (quarks and gluons) inside the colliding hadrons in order to correlate theoretical QCD calculations with experimental data. To zeroth order in α_s, the structure functions

are precisely measured in respect of parton distribution functions (PDFs). In the parton model approximation, the proton is composed of a number of free constituents, each of which carry a fraction x of the protons total momentum. In this framework the structure functions are usually identified by the summation over the incoherent sum of the parton's momentum distributions $q_i(x)$ for each quark flavor i,

$$F_2(x) = 2xF_1(x) = \sum_i e_i^2 x q_i(x), \tag{1.9}$$

where the sum implies summation over all flavours of quarks and antiquarks. e_i is the electric charge of a parton of type i. The functions $q_i(x)$ are known as the PDFs describing the probability of finding a parton of flavor i inside the proton with a longitudinal momentum fraction x at resolution scale Q^2. The proton consists of three valence quark flavors uud along with the many quark-antiquark flavors $u\bar{u}$, $d\bar{d}$, $s\bar{s}$ and so on, known as the 'sea' quarks. As a first approximation, we may assume the three lightest quark flavors u, d and s, having roughly the same fequency and momentum distribution, to occur in the sea and neglect the possibility of sizeable presence of heavier quark flavors. To recover the quantum numbers of proton, the net numbers of quarks need to satisfy the following sum rule:

$$\int_0^1 (u(x) - \bar{u}(x))dx = 2; \int_0^1 (d(x) - \bar{d}(x))dx = 1; \int_0^1 (s(x) - \bar{s}(x))dx = 0, \tag{1.10}$$

resulting charge=+1, baryon no.=1, strangeness=0. Another important sum rule is the momentum sum rule which demands that the sum of the momenta of all partons must be equal to the momentum of the proton, i.e.

$$\sum_i \int_0^1 x q_i(x) dx = 1. \tag{1.11}$$

The PDFs, being non-perturbative, cannot be fully obtained by perturbative QCD. These are rather derived by fitting observables to experimental data. Nevertheless, within QCD one can study the rate of change of the PDFs with the resolution scale Q^2 and it is controlled by the QCD evolution equations for parton densities. As mentioned earlier, QCD predicts a dependence of the structure function on the scale Q^2 induced by corrections in $\alpha_s(Q^2)$ arises from diagrams with real gluon emission. So QCD modifies the F_2 structure function as

$$F_2(x, Q^2) = \sum_i e_i^2 x(q_i(x, Q^2)). \tag{1.12}$$

Thus the structure function as well as the parton distributions now have a Q^2 dependence resulting in scaling violation. The general strategy to determine PDFs is comprised of parametrizing the dependence of the parton distributions on the variable x at some small value of $Q^2 = Q_0^2$, either by constructing a rough presumption on their analytical forms or by employing the neural-net technology, and evolving these input distributions to high Q^2 via the evolution equations. Be that as it may, there is still not a particular set of PDFs commonly acknowledged. Presently the parametrizations of PDFs are accomplished by several groups, mainly the GRV/GJR [31, 32], MRST/MSTW [33-35], NNPDF [36, 37], HERAPDF [38, 39] and CTEQ [40, 41]. We will further discuss these PDFs groups in more detail in section 1.6.2 of this chapter. These groups differ mainly in the input data, the methods of parametrizations, the treatment of heavy quarks and the value of the coupling constant α_s as well the methods of analysis. To comprehend the common features and ambiguity as well as the discrepancies between the predictions of the PDF groups an active association has been set up at CERN in recent times.

1.5 Gluon shadowing at small-x

One of the present most fascinating issues of QCD is the growth of hadronic cross sections at high energies or in other words at small-x. At very high energies hadronic interactions have been manifested to be impelled by states with high partonic densities and accordingly many phenomenological and theoretical efforts have been made to explain it. A vital finding of the past years is the prepotent role of gluons with very small fractional momentum x in nucleons when observed by a high energy probe. Thus increase of energy causes a rapid growth of the gluon density in the limit $x \to 0$ eventually leading to the saturation effects [42-44]. That being so, the study of lepton-nucleon DIS or most importantly the determination of the gluon density in the region of small-x is considerably relevant as it could be a measure of perturbative QCD or a probe of novel effects and further because it is the primary factor in numerous other analysis of different high energy hadronic processes. There have been enormous phenomenological and experimental activities for decades regarding the interpretation of small-x QCD from DIS at HERA to heavy ions collisions at RHIC. Moreover the study of this kinematic regime is of uttermost importance to

compute particle production in the proton-proton collisions at LHC.

The small-x demeanor of structure functions for fixed Q^2 exhibits the high-energy nature of the total cross section with growing total center of mass energy squared s since $s \simeq Q^2(\frac{1}{x} - 1)$ [44]. At very high energies, one can therefore access the region of smaller and smaller values of x. At small-x, the likelihood for the photon of detecting a small-x parton increases and for sufficiently small values of x the virtual photon no longer interacts with each parton deliriously, rather there may be multiple scattering off various partons. However the sharp growth of the gluon density towards small-x will eventually have to slow down in order to restore the Froissart bound [45, 46] on physical cross sections. This bound controls the upper limit for the increase of the cross section at asymptotically large values of s and is established on analyticity and unitarity constraints. The Froissart bound indicates that the total cross section does not grow faster than the logarithm squared of the energy as $s \to \infty$ or, equivalently, as $x \to 0$, i.e., $\sigma_{total} = \frac{\pi}{m_\pi^2}(\ln s)^2$, where m_π measures the range of the strong force. It seems that there should be some process which restricts the growth of the gluon distribution at small-x and subsequently prohibits the cross section from growing very rapidly. Gluon recombination is generally regarded as the mechanism liable for this taming or a potential saturation of the gluon distribution function at very small-x.

As x decreases for fixed Q^2, the number of gluons increases, and at some value of $x = x_{crit}$ the entire transverse area inhabited by gluons turns out to be comparable to or larger than the transverse area of a proton. In consequence, at sufficiently high energy the semi-hard processes, which complements the interactions of gluons with a very small fraction of the proton's momentum, may affluently contend the soft processes [42]. In other words, at very small values of x the number densities of gluons will be so high that the probability of interaction between two gluons can no longer be overlooked. That is to say, at very small-x ($x < x_{crit}$) gluons start to overlap spatially and so the processes of recombination of gluons will be as essential as their emission. In this way the increase in the number of small-x gluons becomes limited by gluon recombination ($gg \to g$) processes which eventually leads to gluon saturation [42, 43, 47]. The phenomena of gluon recombination is also known as absorptive corrections, shadowing, nonlinear effects, screening or unitarity corrections. The gluon saturation

is one of the most fascinating problems of the small-x physics, which is presumed on theoretical basis and there is emerging indications of its existence. The pioneering finding of the geometrical scaling in HERA data [48] as well as the existance of geometrical scaling in the production of comprehensive jets in the LHC data [49] provides strong experimental evidences of the saturation effects.

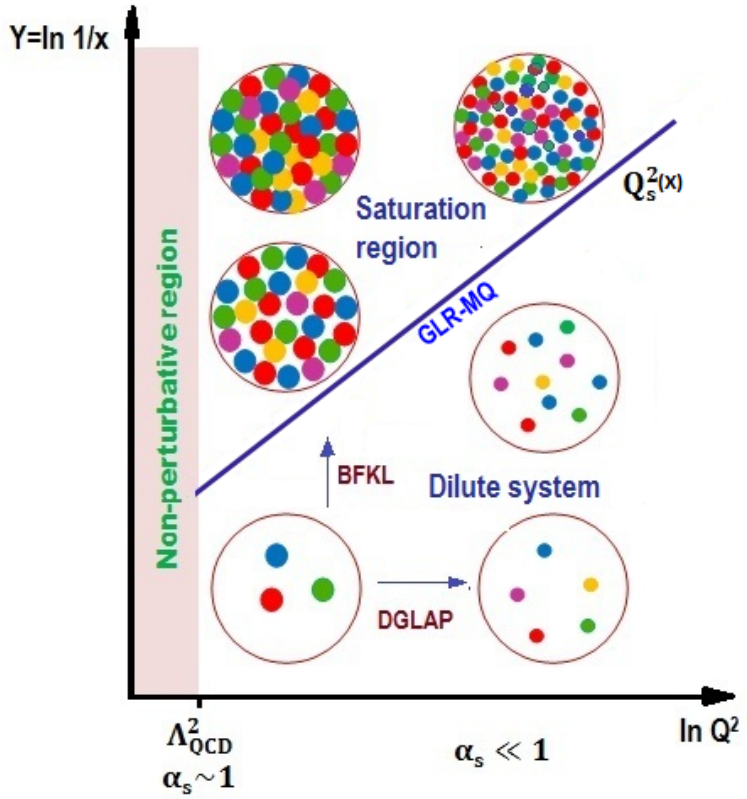

Figure 1.5: Schematic picture of parton saturation

In conjunction with energy the inception of saturation also depends on the size of the gluons, defined as $r \sim 1/Q$ in DIS. With larger sized gluons the available hadron area will be teemed earlier and the gluons start to re-interact whereas, when the size is small the saturation will be deferred to larger energies. The process of gluon saturation is schematically portrayed in Figure 1.5. There is a typical transverse momentum scale Q_s related to saturation which separates the dilute regime from the saturated regime. It is known as the saturation scale and it signifies the scale at which the nonlinear effects become important. Q_s is proportional to the density of gluons per unit area [50]:

$$Q_s^2(x) \simeq \frac{\alpha_s}{N_c} \frac{x g(x, Q^2)}{\pi R^2} \sim x^{-\lambda}, \tag{1.13}$$

where R is the radius of the hadron where gluons populate. The saturation scale is the key parameter in saturation physics [47-54] and grows with $1/x$. Therefore, for sufficiently small-x, $Q_s^2 >> \Lambda^2$ with Λ being the QCD cut off parameter and thus the small coupling approach is legitimate. Below the saturation scale the nonlinear effects begins to decelerate and ultimately saturate the rapid growth of the gluon densities.

The conventional perturbative QCD methods cannot be pertained in the kinematic region of small-x and large-Q^2, where α_s continues to be small but the density of gluons becomes high enough. The interactions among the gluons in this dense system disagree with the fundamental presumption of the QCD improved parton model where the partons are considered to be noninteracting. The physics that controls this high density region is non-perturbative, but of a nature unlike the one analogous to large distances [47, 55]. Nevertheless there is a transition region between perturbative QCD and high density QCD where some aspects of the aforementioned dense system of gluons can be studied and this transition region is likely to analyse through perturbative approach. The linear QCD evolution equations, such as the DGLAP [56-58] and the Balitsky-Fadin-Kuraev-Lipatov (BFKL) [59-61], are therefore expected to breakdown in the kinematic region of very small-x where the gluon recombination processes give rise to nonlinear corrections. A comprehensive study of this region was first performed by Gribov, Levin and Ryskin, and by Mueller and Qiu (GLR-MQ) in their pioneering papers [42, 43] and they suggested that the higher twist phenomena of gluon recombination or shadowing corrections could be expressed in a new evolution equation which is nonlinear in gluon density. This nonlinear evolution equation is nowadays referred to as the GLR-MQ equation. In the recent years various alternative nonlinear evolution equations admissible at high gluon densities have been derived and analysed widely and subsequently the structure functions from DIS or more particularly the PDFs have been investigated in the framework of saturation models. These are the Modified-DGLAP (MD-DGLAP) [62], Balitsky-Kovchegov (BK) [63, 64], Modified-BFKL (MD-BFKL) [65] and Jalilian-Marian-Iancu-McLerran-Weigert-Leonidov-Kovner (JIMWLK) [66, 67]. We present a brief account of these linear and nonlinear QCD evolution equations in Chapter 2 of this thesis.

The picture of high gluon density in QCD can be quantitatively executed by a

crucial parameter [55]

$$\widetilde{W} = \frac{\alpha_s(Q^2)}{Q^2}\rho(x, Q^2), \tag{1.14}$$

which represents the probability of gluon recombination throughout the cascade. Here $\rho = \frac{xg(x,Q^2)}{\pi R^2}$ is the the density of gluons in the transverse plane, $xg(x, Q^2)$ number of gluons per unit of rapidity ($Y = \ln(1/x)$) which interacts with the probe and $\alpha_s/Q^2 \sim \sigma_{gg\to g}$ represents the cross section of gluon-gluon interaction. This parameter controls the precision of calculations involving gluon-gluon interactions. The unitarity constraint on physical cross sections can be expressed as $\widetilde{W} \leq 1$ [55]. In the region of x and Q^2 where $\widetilde{W} << 1$, the interaction of gluons is negligible and we may proceed with the evolution equations linear in gluon density. However, at small-x the gluon density becomes so large that $\widetilde{W}$ can become appreciable in which case higher twist effects of gluon-gluon interactions can no longer be ignored and in that case the evolution is governed by the nonlinear evolution equations. The correlation radius of two interacting gluons is characterized by R and its value depends on how the gluons ladders couple to different partons. If the gluons originate from sources which occupy distinct regions in longitudinal coordinate space then R is of the order of proton radius, i.e. $R = 5$ GeV^{-1} [42]. In that case recombination probability is very negligible. On the other hand, if the gluon ladders couple to the same quark or gluon then the gluons are expected to be concentrated in small areas inside the proton, the so-called hot-spots [43, 68]. Such hot spots of high gluon density can enumerate the rapid onset of gluon-gluon interactions in the environs of the emitting parton and so uplift the recombination effect or shadowing corrections. In such hot spots R is considered to be of the order of the transverse size of a valence quark, i.e. $R = 2$ GeV^{-1}.

Gluon saturation as well as the high parton density regime within hadronic and nuclear wave functions at small-x are properly described in the effective theory of Color Glass Condensate (CGC) [69-71] and related formalisms. It is predicted by the theorists that, when Q_s^2 is large the interactions among the individual gluons are feeble but they jointly form a very strong coherent classical color field analogous to Bose-Einstein condensates and glassy materials, and is therefore marked as the CGC. The CGC is expected to be the universal restrain for the constituents of a comprehensible hadron wave function which is, as a whole, high density of gluons

and for resolving momenta below the saturation scale.

As a general comment, we note that exploring the dynamics of the high density QCD at small-x is one of the current most demanding problems in high energy physics and there has been significant breakthrough formulated to comprehend gluon recombination or shadowing. Numerous theoretical and phenomenological endeavours have been done in the recent years to investigate the saturation phenomena based on perturbative QCD [72-79].

1.6 Experiments and parametrizations

1.6.1 Experiments

The structure functions measurements have been accomplished by several high energy experiments over the past years. The DIS experiments utilizing charged and neutral lepton beams have steadily enhanced the understanding of the structure functions in recent years. The first electron-proton DIS experiments were performed at SLAC in 1968 in California [80]. Following this the progress of the E26 [81], CHIO [82], Bologna-CERN-Dubna-Munich-Saclay (BCDMS) [83], European Muon Collaboration (EMC) [84], New Muon Collaboration (NMC) [85] and E665 [86] muon scattering experiments at Fermilab and CERN, and the HERA [27-30, 87] at DESY have been established in the past years. These muon scattering experiments were improved by a course of high energy neutrino scattering experiments as well at Fermilab and CERN. The most recent high energy experiments of p-p collisions are the Large Hadron Collider (LHC) [88, 89] which is the latest addition to CERN's accelerator complex. The LHC is the biggest and most complicated experimental facilities ever constructed and is likely to confront some of the unanswered queries of physics, promoting knowledge of physical laws. A brief account of some of these experiments are given below.

SLAC

The SLAC experiments were fixed target experiments operated during the time period from 1968 to 1985 using 21 GeV electrons scattered off hydrogen and deuterium targets. The first DIS experiments exploring the proton structure were performed at SLAC in 1968. The SLAC measurements [80] covered a kinematic range

$0.06 \leq x \leq 0.9$ and $0.6 \leq Q^2 \leq 30$ GeV^2. The overall normalization error of the experiments is about 2.1%. The structure function F_2 was obtained using R_{SLAC}, where R is the ratio of the longitudinally polarized virtual photon absorption cross section to that of transversely polarized.

BCDMS

The BCDMS experiment (NA4) at CERN ran parallel to EMC from 1978 up to 1985 and included a DIS of muons on a hydrogen target using beams of 100, 120, 200 and 280 GeV. The the kinematic range covered in these measurements is [83] $0.06 \leq x \leq 0.8$ and $7 \leq Q^2 \leq 260$ GeV^2. The structure function F_2 was extracted using R_{QCD} and an overall normalization error is around 3% was reported.

EMC

The EMC experiment (NA28) at CERN was performed using a beam of 280 GeV muons on a deuterium as well as heavier elements target. The kinematic range $0.0025 \leq x \leq 0.14$ and $0.25 \leq Q^2 \leq 7.2$ GeV^2 provided a good description of the measurements [84] whereas the rest of their measurements is superseded by the more precise measurements of NMC described below. There is an overall normalization error of 7%. The F_2 structure function was obtained using R_{CHIO} of CHIO collaboration.

NMC

The NMC-NA37 experiment was an extension of the EMC experiment with an upgraded apparatus performed by the new muon collaboration at the M2 muon beam line of the CERN SPS. This experiment measured simultaneously the proton and deuteron differential cross sections using two similar pairs of 3 m long targets exposed off and on to the muon beam and these measurements considerably reduced the uncertainty of the relative normalization between the proton and deuteron structure functions. An overall normalization error of 2% is claimed. An iterative method based on a Monte Carlo simulation of the experiment was applied to determine the structure functions. For each period of data taking individual simulations were performed to allow changes in the beam and the detector to be considered. The values of $F_2(x, Q^2)$ were obtained performing a comparison of the normalized outputs of data

and accepted Monte Carlo events. The structure functions were computed from an initial selection of F_2 and a fixed parametrization of the ratio, $R(x, Q^2)$, obtained from a global analysis of SLAC data [80]. The proton and deuteron structure functions F_2^p and F_2^d were measured in the kinematic range $0.006 < x < 0.6$ and $0.5 < Q^2 < 75$ GeV^2, by inclusive DIS with beams of 90, 120, 200 and 280 GeV muons on hydrogen and deuterium targets [85].

E665

The E665 experiment at Fermilab is a fixed-target muon scattering experiment, with the highest energy of about 490 GeV muon beams. The E665 experiment took data using liquid hydrogen and deuterium targets, as well as heavy targets and measured the structure functions and their ratios as well as investigated the hadronic final states produced in the muon interaction. The F_2 measurements are reported in the kinematic range $8.9 \times 10^{-4} \leq x \leq 0.39$ and $0.2 \leq Q^2 \leq 75$ GeV^2 [86]. The overall normalization error is of 1.8%. There is a significant overlap in x and Q^2 of the E665 measurements with those of NMC and the two measurements are accorded well in the region of overlap. The E665 data being at lower Q^2 at fixed x, these measurements overlap in x with the HERA data as well. Like NMC, the E665 analysis of F_2 also use the parametrization of R obtained from a global analysis of SLAC data [80].

H1 and ZEUS

H1 and ZEUS are the two major experiments at the particular lepton-proton collider HERA, hosted by DESY in Hamburg, Germany to investigate the DIS processes. H1 is an international collaboration involving about 250 scientists from 20 institutes and 12 countries whereas ZEUS collaboration is handled by 450 physicists from 12 countries, forming it a genuinely international scientific collaboration. The outset of operation of the HERA collider provides an important landmark for the measurements of the proton structure. Both the H1 and ZEUS experiments at HERA have measured the inclusive $e^{\pm}p$ NC and CC DIS cross sections. HERA collides 920 GeV protons off 27.5 GeV electrons inducing a large center of mass energy of the collisions $\sqrt{s} \approx 320$ GeV. The maximum value of Q^2 at H1 and ZEUS experiments measures to $90,200$ GeV^2 whereas the calibrated x-range have been remarkably extended to a smaller value of $x \sim 10^{-5}$ [27-30, 87]. The operation of HERA have been carried out

in two stages, HERA-I, from 1992-2000, and HERA-II, from 2002-2007. The utmost precise determination of the proton structure is measured by the H1 and ZEUS collaborations using the HERA-I data. During the HERA-I period, HERA was mostly operating with positrons due to restrictions of the electron beam life time. However this problem has been resolved for HERA-II and during the period from 2004 to 2006 HERA operated with electron beams allowing a more precise measurement of the xF_3 structure function. In the year 2007, HERA performed a series of runs with lowered proton beam energies of 460 and 575 GeV producing data sets essential for the first direct measurement of F_L. The H1-ZEUS combined results [87] have reduced the uncertainties to a large extent compared to the individual experiments and act as a basis for a precise fit of the proton PDFs. In both experiments the structure function F_2 was extracted using R_{QCD}. The kinematic range of the NC data is $6 \times 10^{-7} \leq x \leq 0.65$ and $0.045 \leq Q^2 \leq 30000$ GeV^2, for values of inelasticity y between 0.005 and 0.95. On the other hand, the kinematic range of the CC data is $1.3 \times 10^{-2} \leq x \leq 0.40$ and $300 \leq Q^2 \leq 30000$ GeV^2, for values of y between 0.037 and 0.76. The total uncertainty of the combined data set is 1% for NC scattering in the region $20 < Q^2 < 100$ GeV^2. Even though HERA ended its 15 years of operation in 2007, dynamic analyses of full data sets are continuing and outstanding improvements are being generated.

LHC

The LHC is the world's largest and most powerful particle accelerator, built by CERN in collaboration with over 10,000 scientists and engineers from over 100 countries, as well as hundreds of universities and laboratories. The LHC weighs more than 38,000 tonnes and runs for 27 km in a circular tunnel 100 metres beneath the Swiss-French border at Geneva, Switzerland. The LHC started up on 2008 successfully circulating the proton beams in the main ring of the LHC for the first time, but stopped operating due to a faulty electrical connection. However in 2009 LHC successfully circulated the proton beams with the first reported p-p collisions at the injection energy of 450 GeV per beam. In 2010 two 3.5 TeV proton beams were made to collide, which is a world history for the highest-energy artifial particle collisions. In 2013 LHC went into shutdown and planned to reopen in early 2015 upgrading the

beam energy to 13 TeV, which is almost double its current maximum energy and more than seven times any predecessor collider. As of 2012 data from over 3×10^{14} LHC proton-proton collisions had been analyzed LHC and the LHC Computing Grid, which provide global computing resources to store, distribute and analyse the ~ 30 Petabytes of data annually generated by the LHC, had become the world's largest computing grid. There are seven experiments at the LHC analysing the innumerable particles produced in the accelerator. The biggest of these experiments, A Toroidal LHC Apparatus (ATLAS) and the Compact Muon Solenoid (CMS), use two independently designed general-purpose detectors to explore a vast range, from the search for the Higgs boson to extra dimensions and dark matter. ALICE (A Large Ion Collider Experiment) is a heavy-ion detector on the LHC ring designed to investigate the formation of the quark-gluon plasma. The purpose of LHC beauty (LHCb) experiment is to study the differences between matter and antimatter. The Total Elastic and diffractive cross section Measurement (TOTEM) and LHC forward (LHCf) experiments study forward particles, protons or heavy ions, and focus on physics that cannot be accessed in the general-purpose experiments. The Monopole and Exotics Detector at the LHC (MOEDAL) approved in 2010 uses detectors to search directly for the magnetic monopole. In 2012, the ATLAS and CMS experiments at LHC announced the observation of a new particle in the mass region around 126 GeV [88, 89]. Later the new particle is confirmed to be the Higgs boson [13] which physicists have been looking for since its prediction about 50 years ago. It is one of the greatest discoveries of the present-day and the Nobel Prize in Physics 2013 was undoubtedly awarded jointly to F. Englert and P. W. Higgs for the theoretical prediction of the Higgs mechanism.

1.6.2 Parametrizations

The PDFs are one of the basic ingredients for the calculation of any observable involving hadrons. The evolution of PDFs is a sensitive test of our understanding of QCD dynamics, which is expressed in the form of PDF evolution equations. Precise knowledge of these PDFs is an essential prerequisite for the identification of any possible signature from physics beyond the SM. On the other hand an accurate evaluation of the errors associated with the PDFs is crucial to generate reliable phe-

nomenological predictions at hadronic colliders, such as the LHC. In Recent times, a substantial amount of theoretical and experimental endeavour has been devoted in the accurate determination of the parton distributions of the nucleon. Particular interests are given in the calculation of the uncertainties associated with various experimental and theoretical inputs, for the sake of precise measurement of collider processes as well as determination of QCD parameters. At present, the preeminent inclusive PDF sets are acquired from a global analysis of hard-scattering data from various processes like DIS, DrellYan, weak vector boson production as well as collider jet production. In global analysis the PDFs are determined unfolding the experimentally measurable structure functions in terms of their parton content, by using the QCD factorization and DGLAP evolution equations. Modern PDFs are constantly developed to incorporate looming theoretical improvement and the most recent data from hadronic experiments. There are various groups extracting PDFs from global data analyses. The LHAPDF [90] library provides a merged and simple computing to all the major PDF sets. The following is a brief description of the major PDF sets available.

GRV/GJR

The GRV global parametrization is a dynamically generated PDFs set advocated by M. Gluck, E. Reya and A. Vogt. defined upto NLO in the $\overline{MS}$ scheme. The GRV group systematically analyze hard scattering data within the framework of perturbative QCD and is very successful in predicting the rapid rise of proton structure function F_2 at small-x, observed at HERA. The GRV1992 PDFs include u, d, s, c and b quarks whereas the GRV1994 include only u, d and s quarks. These PDFs are used in the calculations involving heavier quarks, with non-zero quark masses, in the partonic hard scattering cross section. The GRV1998 global parametrization [31] used H1 and ZEUS high precision data and presents an updated, more accurate, version of valence-like dynamical input distributions. The GRV1998 PDFs compute the light-parton distributions, charm and bottom contributions to F_2 and the scale dependence of α_s in NLO and LO. The parton densities and the F_2 structure functions are determined from interpolation networks covering the regions $0.8 < Q^2 < 10^6$ GeV^2 and $10^{-9} < x < 1$. Moreover, perturbatively fixed parameter-free dynam-

ical prognostications for parton distributions are unfolded to the very small-x region, $10^{-8} \leq x \leq 10^{-5}$ [31], enabling fairly decent evaluations of ultra high energy neutrino-nucleon cross section concerning neutrino astronomy. The LO results corresponds to $\Lambda_{LO}^{(N_f=4)}$=175 MeV which leads to the value of $\alpha_s^{LO}(M_Z^2)$=0.125. The resulting LO input distributions at $Q^2 = \mu_{LO}^2 = 0.26$ GeV^2 for gluon is given by $xg(x, Q^2) = 17.47x^{1.6}(1-x)^{3.8}$. On the other hand the NLO results correspond to $\Lambda_{NLO}^{(N_f=4)}$=246 MeV giving rise to the value of $\alpha_s^{NLO}(M_Z^2)$=0.114. The input distributions have been established employing the 1994 and 1995 HERA F_2^p results [27-30] as well as the fixed target F_2^p data of SLAC, BCDMS, NMC and E665.

The GJR parametrization [32], recommended by M. Gluck, P. Jimenez-Delgado and E. Reya, is the upgraded version of GRV1998 parton distributions. The GJR dynamical distributions generated the small-x ($x \leq 10^{-2}$) structure of dynamical parton distributions from valence-like initial distributions considered at input scale $Q_0 < 1$ GeV. It provides assurance in the trustworthy prediction of the cross sections for heavy quark, $W^{\pm}$, Z_0, and high p_t jet production at the the hadron colliders such as Tevatron and LHC. On the other hand, in the JR09 parametrization [91] the previous LO and NLO global fit analyses for the dynamical parton distributions of the nucleon are extended to NNLO of perturbative QCD utilizing the DIS structure function measurements as well as the hadronic Drell-Yan dilepton production data.

MRST/MSTW

The MRST is a global analysis of parton distributions of the proton recommended by A. D. Martin, R. G. Roberts, W. J. Stirling and Robert Thorne in the $\overline{MS}$ renormalization scheme. MRST2001 PDFs [33] execute a global parton analysis up to NNLO incorporating all the convenient explicit data from DIS and similar hard scattering processes viz. H1, ZEUS, BCDMS, NMC, E665, SLAC and CCFR. This PDFs set is ordinarily suitable to DIS data with $Q^2 > 2$ GeV^2 and $W^2 > 10$ GeV^2, however it concedes the HERA data for Q^2 down to 1.5 GeV^2 to cover the very small-x calculations of F_2. The initial parametrization of the gluon for LO is $xg = 3.08x^{0.10}(1-x)^{6.49}(1-2.96x^{0.5}+9.26x)$, for $\alpha_s(M_Z^2)$=0.130 and $\Lambda_{\overline{MS}}(N_f=4)$=220 MeV [33]. The best global NLO fit is achieved with the initial distribution of the gluon at Q_0^2= 1 GeV^2 and it complements to $\alpha_s(M_Z^2)$=0.119, i.e. $\Lambda_{\overline{MS}}(N_f=4) = 323$ MeV.

These data sets permits the developement of negative input gluon parametrization at small-x. The optimum global NNLO fit is acquired considering the input distribution of the gluon at Q_0^2=1 GeV^2 conforming to $\alpha_s(M_Z^2) = 0.1155$, i.e. $\Lambda_{\overline{MS}}(N_f = 4) = 235$ MeV. The MRST2004 parton sets [34] provide an additional physical parametrization of the gluon distribution for global parton analysis at both NLO and NNLO thereby producing an improved illustration of the W and Z production cross sections at the Tevatron and the LHC in contrast to the earlier set. The complete kinematic domain covered by this PDF sets, where fixed-order DGLAP analysis is convenient, including the corresponding sets of traditional partons, is found to be $W^2 > 15$ GeV^2, $Q^2 > 10$ GeV^2 and $x > 0.005$ at NLO, whereas at NNLO it is given by $W^2 > 15$ GeV^2, $Q^2 > 7$ GeV^2 and $x > 0.005$.

The MSTW2008 [35] is an updated LO, NLO and NNLO PDFs calculated from global analysis of hard scattering data in the $\overline{MS}$ scheme. The MSTW2008 global analysis supersedes all the previous MRST sets and is very convenient in forecasting the accuracy of cross sections and related theoretical calculations of W and Z bosons, Higgs boson and inclusive jet production at the Tevatron and uncertainties at the LHC. This PDFs fit include CCFR/NuTeV di-muon cross sections and Tevatron Run II data on inclusive jet production. Together with α_s there are 30 free PDF parameters in the fit. The MSTW analysis, fits ~ 2700 data points as a whole and the comprehensive nature of the NLO and NNLO fits is identical and perfectly admissible, with $\chi^2/N_{pts} \sim 1$ for nearly all data sets [35]. This fit furthermore determines the uncertainty on the strong coupling α_s, owing to the experimental errors on the data, which is found to be $\alpha_s(M_Z^2) = 0.1202^{+0.0012}_{-0.0015}$ at NLO and $\alpha_s(M_Z^2) = 0.1171^{+0.0014}_{-0.0014}$ at NNLO.

NNPDF

The NNPDF approach is based on the application of neural networks as primary interpolating mechanisms. The neural networks can yield an impartial interpolation which produces the measure for all points, in some ways within a finite range of x and Q^2 where the data sampling is excellent. The NNPDF approach bypasses all the problems present in the usual approach to the determination of the PDFs. These PDF fits determine the probability density in the arena of structure functions for the

proton, deuteron and nonsinglet structure functions calculated from experimental data of the NMC, BCDMS, E665, ZEUS and H1 collaborations. Their results adopt the form of a set of 1000 neural nets, each providing a calculation of F_2 for given x and Q^2. The central value and the statistical moments of the structure functions determined in the NNPDF fit can be computed out of the 1000 nets in accordance with the standard Monte Carlo techniques. NNPDF1.0 [36] is a set of parton distributions of the nucleon, at NLO, from a global set of DIS data employed to estimate the standard W and Z cross sections at the LHC. Including the recent neutrino dimuon production data in combination with a global deep inelastic parton fit, the NNPDF1.2 parton set is constructed and it provides a determination of the strange and antistrange distributions of the nucleon. Apart from being a transitional step towards a fully global fit including hadronic data, this set ia an interesting test of the NNPDF methodology and for the determination of electroweak parameters.

NNPDF2.0 [37] global set of PDFs include DIS with the combined HERA-I dataset, fixed target Drell-Yan production, collider weak boson production and inclusive jet production. It also determines the impact of recent high luminosity D0 Run II lepton asymmetry data and the D0 inclusive muon and electron data. These PDFs sets are very advantageous to the experimentalists in all kinds of circumstances, for example, examining the accuracy of preliminary datasets and their uncertainties, evaluating the validity of viable evidences of new physics, or in improving the design of new experiments using pseudo data. This fit is upgraded to NNPDF2.1 set to including the heavy quark mass effects. These data sets take care of the small-x gluon and are sensitive to the value of the charm mass m_c as well.

HERAPDF

The HERAPDF project determines the quark and gluon distribution functions of the proton from experimental data and has established a statistical combination procedure enhancing the estimation of the average of H1 and ZEUS measurements in a model independent way. The HERAPDF analysis also elucidates the correlated systematic ambiguities enabling cross calibration to lessen the total systematic uncertainty on the combined data. Thereupon the averaged data are utilized in a QCD fit to determine the proton PDFs with an exhaustive interpretation of the experimental

and theoretical uncertainties. HERAPDF0.1 [38] set is a NLO QCD analysis of parton distributions and covers the combined data set of the inclusive deep inelastic cross sections measured by the H1 and ZEUS Collaborations in NC and CC unpolarised $e^{\pm}p$ scattering at HERA. In this analysis the PDFs are parametrized at the starting scale of $Q_0^2 = 4$ GeV^2 and are evolved using the DGLAP evolution equations.The HERAPDF1.0 [39, 92] analysis employs a uniform data set with small associated systematic uncertainties and applies the conventional χ^2 tolerance, $\Delta\chi^2 = 1$ to determine the experimental uncertainties on the PDFs. On account of the precision of the combined data set, the total uncertainties of the HERAPDF1.0 parametrization is of the order of a few percent at small-x, which is much improved compared to the earlier extractions of the PDFs using the individual H1 or ZEUS data. The gluon distribution functions are parametrized by the universal form $xg(x) = A_g x^{B_g}(1-x)^{C_g}$ at the input scale $Q_0^2 = 1.9$ GeV^2, so that $Q_0^2 < m_c^2$ [38]. A_g is the normalization parameter, B_g represents the small-x behaviour whereas C_g represents the high-x behaviour.

The HERAPDF1.0 set has been amended to HERAPDF1.5 by incorporating initial all-inclusive cross section data from HERA-II running. On the other hand the HERAPDF1.6 analysis involves the H1 and ZEUS jet data whereas HERAPDF1.7 fit comprises of all the data sets from HERA-I and II, charm data, low energy data and jet data. Moreover the NLO fits have been continued to NNLO for both HERAPDF1.0 and HERAPDF1.5 [39, 92]. The HERAPDF1.0 NNLO parton set was introduced in 2010 but this has been upgraded to HERAPDF1.5NNLO fit which has an essentially vigorous high-x gluon and provides thorough description of the experimental, model and parametrization uncertainties. The prescribed value for $\alpha_s(M_Z)$ at NNLO is $\alpha_s(M_Z) = 0.1176$ [39]. These HERAPDFs have been affluently encountered both the Tevatron and LHC data on W, Z and jet production.

CTEQ

The CTEQ global QCD analyses of PDFs have been developed over decades. The CTEQ series include CTEQ1, CTEQ2, CTEQ3, CTEQ4, CTEQ5 presented during the period from 1993 to 2000, followed by sets of CTEQ6 published in the period from 2002 to 2006 as well as the ensuing PDF sets CT09 [40, 93-95]. Recently in 2010

CTEQ group presented NLO PDFs named as CT10 and CT10W [40]. These two new PDF sets are built on the contemporary knowledge of the PDFs obtained from global hadronic experiments, mainly the DIS combined data set of HERA-1 cross sections, which supersedes 11 separate HERA-1 data sets, considered in CTEQ6.6 and preceding fits. These PDFs sets have been used in a broad way in phenomenological predictions for the Tevatron, LHC, and other experiments. The CT10 global QCD fits involve a combination of DIS cross sections by the H1 and ZEUS collaborations in HERA-1, measurements of the charge asymmetry of leptons from W boson, Z rapidity distributions, single-inclusive jet cross sections by CDF as well as DØ collaborations at the Tevatron. The CT10 PDFs are derived at NLO in α_s, incorporating the general-mass analysis of charm and bottom quark contributions to hadronic observables. The CT10 NLO QCD analysis is in general compatible with the HERA experiments in the region $Q > 2$ GeV. The net consistency of the CT10 fit with the combined H1 data is somewhat poor than with the separate H1 data sets, due to some increase in $\chi^2/d.o.f.$ for the NC DIS data at $x < 0.001$ and $x > 0.1$ [40]. Both CT10 and CT10W PDF sets contain 26 independent parameters and thus there are 26 eigenvector directions and a total of 52 error sets. These PDF error sets, together with the following α_s error sets, admit a thorough computation of the combined PDF+α_s uncertainties for any observable. Both CT10 and CT10W predict a minor PDF inspired uncertainty in the total cross section for the top-quark pair production at the Tevatron Run-II in contrast to the CTEQ6.6 prediction. The difference between the CT10 and CT10W PDF sets for LHC predictions is very negligible, other than in those observables that are responsive to the ratio of down-quark to up-quark PDFs.

The CT10NNLO [41] global PDF fit is the NNLO analysis of the PDFs recently published by the CTEQ group. It includes basically the same global data sets used in the CT10 and CT10W NLO PDF fits excluding the Tevatron Run-1 inclusive jet data and a subset of the Tevatron Run-2 lepton charged asymmetry data from W boson decays. This fit produces numerous predictions at NNLO precision for both current and upcoming precision measurements from the LHC at CERN. It further analyzes the extent of variations in the gluon distributions initiated by corresponding systematic effects in inclusive jet production.

1.7 Outline of the thesis

This thesis is concerned with the linear DGLAP and nonlinear GLR-MQ evolution equations in the small-x kinematical region and the saturation of gluon density at very small-x due to nonlinear or shadowing corrections to the QCD evolution at very small-x. We present a review of different QCD evolution equations both linear and nonlinear in Chapter 2. Part I of this thesis details the study of the linear DGLAP equation. In chapter 3 we report the semi-numerical solution of the DGLAP equation in the small-x limit for singlet structure functions at LO, NLO and NNLO. The Q^2 and x-dependence of the singlet structure functions have been examined from these solutions and the results are compared with different experimental data and parametrizations. Following this in chapter 4 we extend the study for gluon distribution function by solving the linear DGLAP equation for gluon distribution analytically. The Q^2 and x-dependence of the gluon distribution functions have been obtained upto NNLO.

In part II we turn our attention to the gluon recombination processes which lead to nonlinear corrections to the linear DGLAP evolution equations due to multiple gluon interactions at very small-x. We estimate the importance of the corrections of these higher order QCD effects, which suppress or shadow and eventually saturate the growth of the parton densities in the framework of nonlinear GLR-MQ evolution equation. We solve this equation for both singlet structure and gluon distribution functions in the vicinity of saturation employing the well-known Regge-like ansatz. In chapter 5 we make a deliberate attempt to explore the effect of shadowing corrections to the behaviour of gluon distribution function in the kinematic region of small-x and Q^2 using the nonlinear GLRMQ evolution equation with the shadowing term incorporated. Our predictions are compared with those obtained by the global QCD fits to the parton distribution functions. Moreover we estimate the effect of nonlinearity in our predictions by comparing the results obtained from nonlinear GLR-MQ equation with those obtained from linear DGLAP equation. Chapter 6 is devoted to the study of the singlet structure function with nonlinear or shadowing corrections in the small-x region based on GLR-MQ equation. The obtained results are compared with different experimental data and parametrizations. A comparative study of our results of nonlinear gluon density with those of other nonlinear equations

is accomplished in chapter 7.

Finally, in chapter 8 we give a brief summary and an outlook for future work.

Bibliography

[1] Ball P., *The Elements: A Very short introduction*, Oxford University Press, Oxford, 2004.

[2] Gell-Mann, M. A schematic model of baryons and mesons, *Phys. Lett.* **8**(3), 214 −− 215, 1964.

[3] Zweig, G. An SU(3) Model for strong interaction symmetry and its breaking: II, *CERN Report* **8419/TH.412**, 1964.

[4] Feynman, R. P. *Photon-hadron interactions*, Addison-Wesley Pub. Co.,Boston, 1972.

[5] Aaij, R., et al. Observation of the resonant character of the $Z(4430)^-$ State, *Phys. Rev. Lett.* **112**(22), 222002, 2014.

[6] Oerter, R. *The theory of almost everything: The standard model, the unsung triumph of modern physics*, Kindle ed., Penguin Group., USA, 2006.

[7] Glashow, S.L. Partial-symmetries of weak interactions, *Nucl. Phys.* **22**(4), 579−−588, 1961.

[8] Weinberg, S. A model of Leptons, *Phys. Rev. Lett.*, **19**(21), 1264−−1266, 1967.

[9] Salam, A. Weak and electromagnetic interactions -in elementary particle theory: relativistic groups and analyticity, Proceedings of the eighth Nobel symposium, N. Svartholm, ed. Almqvist & Wiksell, 367-377 (1968).

[10] Arnison, G. et al., Experimental observation of isolated large transverse energy electrons with associated missing energy at $s = 540$ GeV *Phys. Lett. B* **122**(1), 103−−116, 1983.

[11] Abe, F. et al., Observation of top quark production in $p\bar{p}$ collisions with the Collider Detector at Fermilab *Phys. Rev. Lett.* **74**(14), 2626−−2631, 1995.

[12] Kodama, K. et al., Observation of tau neutrino interactions, *Phys. Lett. B* **504**(3,) 218−−224, 2001.

[13] Cho, A. Higgs boson makes its debut after decades-long search, *Science* **337**(6091), 141−−143, 2012.

[14] Accardi, A. et al., Electron Ion Collider: The next QCD frontier - Understanding the glue that binds us all, *arXiv:1212.1701v3* [nucl-ex].

[15] Gross, D. J. and Wilczek, F. Asymptotically free gauge theories. 1, *Phys. Rev. D* **8**(10), 3633, 1973.

[16] Gross D. J. and Wilczek, F. Asymptotically free gauge theories. 2, *Phys. Rev. D* **9**(4), 980, 1974.

[17] Politzer, H. D. Asymptotic Freedom: An approach to strong interactions, *Phys. Rept.* **14**(4), 129, 1974.

[18] Halzen, F. and Martin, A. D. *Quarks and Leptons: An Introductory course in modern particle Physics*, John Wiley and Sons, Canada, 1984.

[19] Fritzsch, H., Gell-Mann, M. and Leutwyler, H. Advantages of the color octet gluon picture, *Phys. Lett. B* **47**(4), 365−−368, 1973.

[20] Prosperi, G. M., Raciti, M. and Simolo, C. On the running coupling constant in QCD, Prog. Part., *Nucl. Phys.* **58**(2), 387−−438, 2007.

[21] Feynman, R. P. Very high-energy collisions of hadrons, *Phys. Rev. Lett.* **23**(24), 1415−−1417, 1969.

[22] Bjorken, J. D. and Paschos, E. A. Inelastic electron-proton and γ-proton scattering and the structure of the nucleon, *Phys. Rev.* **185**(5), 1975−−1982, 1969.

[23] Abelleira Fernandez, J. L. et al., A Large Hadron Electron Collider at CERN: Report on the physics and design concepts for machine and detector, *J.Phys. G: Nucl. Part. Phys.* **39**(7), 075001, 2012.

[24] Bjorken, J.D. Asymptotic sum rules at infinite momentum, *Phys. Rev.* **179**(5), 1547−−553, 1969.

[25] Abbott, L. F., Atwood, W. B. and Michael Barnett, R. Quantum-chromodynamic analysis of eN deep-inelastic scattering data, *Phys. Rev. D* **22**(3), 582−−594, 1980.

[26] Adler, S. L. and Tung, W. Breakdown of Asymptotic sum rules in perturbation theory, *Phys. Rev. Lett.* **22**(18), 978−−981, 1969.

[27] Adloff, C. et al., On the rise of the proton structure function F_2 towards low x, *Phys. Lett. B* **520** (3-4), 183−−190, 2001.

[28] Adloff, C. et al., Measurement and QCD analysis of neutral and charged current cross sections at HERA, *Eur. Phys. J. C* **30**(1), 1−−32, 2003.

[29] Breitweg, J. et al., Measurement of the proton structure function F_2 and $\sigma_{tot}^{\gamma p}$ at low Q^2 and very low x at HERA, *Phys. Lett. B* **407**(3-4), 432−−448, 1997.

[30] Chekanov, S. et al., High-Q^2 neutral current cross sections in e^+p deep inelastic scattering at $\sqrt{s} = 318$ GeV, *Phys. Rev. D* **70**(5), 052001, 2004.

[31] Gluck, M., Reya, E. and Vogt, A. Dynamical parton distributions revisited, *Eur. Phys. J. C* **5**(461), 470, 1998.

[32] Gluck, M. Jimenez-Delgado, P. and Reya, E. Dynamical parton distributions of the nucleon and very small-x physics, *Eur. Phys. J. C* **53**(3), 355−−366, 2008.

[33] Martin, A.D. et al., NNLO global parton analysis, *Phys. Lett. B* **531**(3-4), 216−−224, 2002.

[34] Martin, A.D. et al., Physical gluons and high-E_T jets, *Phys. Lett. B* **604**(1-2), 61−−68, 2004.

[35] Martin, A.D. et al., Parton distributions for the LHC, *Eur.Phys.J. C* **63**(2), 189−−285, 2009.

[36] Ball, R. D. et al., A determination of parton distributions with faithful uncertainty estimation, *Nucl. Phys. B* **809**(1-2), 1−−63, 2009.

[37] Ball, Richard D. A first unbiased global NLO determination of parton distributions and their uncertainties, *Nucl. Phys. B* **838**(12), 136−−206, 2010.

[38] Kretzschmar, J. Proton structure measurements and the HERAPDF fit, *arXiv:0906.1108* [hep-ex].

[39] Cooper-Sarkar, A. PDF Fits at HERA, *arXiv:1112.2107* [hep-ph].

[40] Lai, H-L. et al., New parton distributions for collider physics, *Phys. Rev. D* **82**(7), 074024, 2010.

[41] Gao, J. et al., CT10 next-to-next-to-leading order global analysis of QCD, *Phys. Rev. D* **89**(3), 033009, 2014.

[42] Gribov, L. N., Levin, E. M. and Ryskin, M. G. Semihard processes in QCD, *Phys. Rep.* **100**(1-2), 1−−150, 1983.

[43] Mueller, A.H. and Qiu, J. Gluon recombination and shadowing at small values of x, *Nucl. Phys. B* **268**(2), 427−−452, 1986.

[44] Kwiecinski, J. Theoretical issues of small x physics, *J. Phys. G: Nucl. Part. Phys.* **22**(6), 685−−702, 1996.

[45] Froissart, M. Asymptotic behavior and subtractions in the Mandelstam representation, *Phys. Rev.* **123**(3), 1053−−1057, 1961.

[46] Martin, A. Unitarity and high-energy behavior of scattering amplitudes, *Phys. Rev.* **129**(3), 1432−−1436, 1963.

[47] Laenen, E. and Levin, E. A new evolution equation, *Nucl. Phys. B* **451**(1-2), 207−−230, 1995.

[48] Iancu, E. and McLerran, L. Saturation and universality in QCD at small x, *Phys.Lett. B* **510**(1-4), 145−−154, 2001.

[49] Collins, J. and Kwiecinski, J. Shadowing in gluon distributions in the small-x region, *Nucl. Phys. B.* **335**(1), 1−−260, 1990.

[50] Levin, E., CGC, QCD, Saturation and RHIC data (Kharzeev-Levin-McLerran-Nardi point of view), *Journal of Physics: Conference Series* **5**(1), 127−−147, 2005.

[51] Stasto, A. M., Golec-Biernat, K. and Kwieciski, J. Geometric scaling for the Total $\gamma^* p$ Cross Section in the Low x Region, *Phys. Rev. Lett.* **86**(4), 596, 2001.

[52] McLerran, L. and Praszalowicz, M. Saturation and scaling of multiplicity, mean p_T and p_T distributions from 200 GeV $\leq \sqrt{s} \leq$ 7 TeV, *Acta Phys. Pol. B* **41**(8), 1917−−1926, 2010.

[53] Mueller, A.H. Small-x behavior and parton saturation: A QCD model, *Nucl. Phys. B* **335**(1), 115−−137, 1990.

[54] Bartels, J. Parton evolution and saturation in deep inelastic scattering, *Eur. Phys. J. C* **43**(1-4), 3−−7, 2005.

[55] Laenen, E. and Levin, E. Parton densities at high energy, *Annu. Rev. Nucl. Part. Sci.* **44**, 199−−246, 1994.

[56] Gribov, V.N. and Lipatov, L.N. Deep inelastic $e-p$ scattering in perturbation theory, *Sov. J. Nucl. Phys.* **15**(4), 438−−450, 1972.

[57] Dokshitzer, Y.L. Calculation of structure functions of deep-inelastic scattering and e^+e^- annihilation by perturbation theory in quantum chromodynamics, *Sov. Phys. JETP* **46**(4), 641−−652, 1977.

[58] Altarelli, G. and Parisi, G. Asymptotic freedom in parton language, *Nucl. Phys. B* **126**(2), 298−−318, 1977.

[59] Lipatov, L.N. Reggeization of the vector meson and the vacuum singularity in Nonabelian Gauge Theories, *Sov. J. Nucl. Phys.* **23**, 338−−345, 1976.

[60] Kuraev, E. A., Lipatov, L. N. and Fadin, V. S. The pomeranchuk singularity in nonabelian gauge theories, *Sov. Phys. JETP* **45** (2), 199−−204, 1977.

[61] Balitsky, I.I. and Lipatov, L.N. The pomeranchuk singularity in quantum chromodynamics, *Sov. J. Nucl. Phys.* **28**, 822−−829, 1978.

[62] Zhu, W. A new approach to parton recombination in the QCD evolution equations, *Nucl. Phys. B* **551**(1-2), 245−−274, 1999.

[63] Balitsky, I. Operator expansion for high-energy scattering, *Nucl. Phys. B* **463**(1), 99−−157, 1996.

[64] Kovchegov, Y. V. Small-x F_2 structure function of a nucleus including multiple Pomeron exchanges, *Phys. Rev. D* **60**(3), 034008, 1999.

[65] Zhu, W., Shen, Z. and Ruan, J. A new perspective on gluon distribution at small x, *arXiv:hep-ph/0703309v4*, 2008

[66] Jalilian-Marian, J. et al., The intrinsic glue distribution at very small x, *Phys. Rev. D* **55**(9), 5414−−5428, 1997.

[67] Jalilian-Marian J. et al., The Wilson renormalization group for low x physics: towards the high density regime, *Phys. Rev. D* **59**(1), 014014, 1999.

[68] Levin, E. M. and Ryskin, M. G. High energy hadron collisions in QCD, *Phys. Rep.* **189**(6), 268−−382, 1990.

[69] Iancu, E., Leonidov, A. and McLerran, L. Nonlinear gluon evolution in the color glass condensate: I, *Nucl. Phys. A* **692**(3-4), 583−−645, 2001.

[70] Ferreiro, E. et al., Nonlinear gluon evolution in the color glass condensate: II, *Nucl. Phys. A* **703**(12), 489−−538, 2002.

[71] Gelis, F. et al., The Color Glass Condensate, *Ann. Rev. Nucl. Part. Sci.* **60**, 463−−489, 2010.

[72] Kharzeev, D., Levin, E. and McLerran, L. Parton saturation and N_{part} scaling of semi-hard processes in QCD, *Phys. Lett. B* **561**(12), 93−−101, 2003.

[73] Zhu, W. et al., Contributions of gluon recombination to saturation phenomena, *Phys. Rev. D* **68**(9), 094015:1-11, 2003.

[74] Iancu, E., Itakura, K. and Munier, S. Saturation and BFKL dynamics in the HERA data at small-x, *Phys. Lett. B* **590**(34), 199−−208, 2004.

[75] Levin, E. and Rezaeian, A. H. Gluon saturation and inclusive hadron production at LHC, *Phys. Rev. D* **82**(1), 014022, 2010.

[76] Blaizot, J.P. The status of parton saturation and the CGC, *Nucl. Phys. A* **854**(1), 237−−256, 2011.

[77] Kormilitzin, A., Levin, E. and Miller, J. S. High density QCD and nucleus-nucleus scattering deeply in the saturation region, *Nucl. Phys. A* **859**(1), 87−−113, 2011.

[78] Xiao, B. The search for gluon saturation in pA collisions, *Nucl. Phys. A* **932**, 380−−386, 2014.

[79] Beuf, G. Gluon saturation beyond (naive) leading logs, *Nucl. Phys. A* **932**, 75−−80, 2014.

[80] Whitlow, L. W. et al., Precise measurements of the proton and deuteron structure functions from a global analysis of the SLAC deep inelastic electron scattering cross sections, *Phys. Lett. B* **282**(3-4), 475−−482, 1992.

[81] Chang, C. et al., Observed deviations from scale invariance in high-energy muon scattering, *Phys. Rev. Lett.* **35**(14), 901−−904, 1975.

[82] Gordon, B. A. et al., Measurement of the nucleon structure functions, *Phys. Rev. D* **20**(11), 2645−−2691, 1979.

[83] Benvenuti, A. C. et al., A high statistics measurement of the deuteron structure functions $F_2(x, Q^2)$ and R from deep inelastic muon scattering at high Q^2, *Phys. Lett. B* **237**(3-4), 592−−598, 1990.

[84] Arneodo, M. et al., Measurements of the nucleon structure function in the range $0.002 \leq x \leq 0.17$ and 0.2 Ge$V^2 \leq$ Q2 $\leq$ 8 GeV^2 in deuterium, carbon and calcium, *Nucl. Phys. B* **333**(1), 1−−47, 1990.

[85] Arneodo, M. et al., Measurement of the proton and the deuteron structure functions, F_2^p and F_2^d, *Phys. Lett. B* **364**(2), 107−−115, 1995.

[86] Adams, M. R. et al., Proton and deuteron structure functions in muon scattering at 470-GeV, *Phys. Rev. D* **54**(5), 3006−−3056, 1996.

[87] Aaron, F.D. et al., Combined measurement and QCD analysis of the inclusive $e^{\pm}p$ scattering cross sections at HERA, *JHEP* **2010**(1), 109:1-55, 2010.

[88] Aad, G. Observation of a new particle in the search for the standard model Higgs boson with the ATLAS detector at the LHC, *Phys. Lett. B* **716**(1), 1−−29, 2012.

[89] Chatrchyan S. et al., Observation of a new boson at a mass of 125 GeV with the CMS experiment at the LHC, *Phys. Lett. B* **716**(1), 30−−61, 2012.

[90] http://projects.hepforge.org/lhapdf/.

[91] Jimenez-Delgado, P. and Reya, E. Dynamical NNLO parton distributions, *Phys. Rev. D* **79**(7), 074023, 2009.

[92] Radescu, Voica. Combination and QCD Analysis of the HERA inclusive cross sections, *arXiv:1308.0374*.

[93] Lai, H. L. et al., Global QCD analysis of parton structure of the nucleon:CTEQ5 parton distributions, *Eur. Phy. J. C* **12**(3), 375−−392, 2000.

[94] Pumplin, J. et al., New generation of parton distributions with uncertainties from global QCD analysis, *JHEP* **2002**(JHEP07:012), 1-46, 2002.

[95] Nadolsky, Pavel M. et al., Implications of CTEQ global analysis for collider observables, *Phys. Rev. D* **78**, 013004, 2008.